

1 Monitoring European anthropogenic NO_x emissions from space

2 Ronald J. van der A^{1*}, Jieying Ding^{1*}, Henk Eskes¹

3 ¹Royal Netherlands Meteorological Institute (KNMI), De Bilt, The Netherlands

4

5 *Corresponding authors: Ronald van der A (avander@knmi.nl), Jieying Ding (jieying.ding@knmi.nl)

6

7 Abstract

8 Since the launch of TROPOMI on the S5p satellite, NO₂ observations have become available
9 with a resolution of 3.5x5 km, which makes monitoring NO_x emissions possible at the scale of
10 city districts and industrial facilities. For Europe, emissions are reported on an annual basis for
11 country totals and large industrial facilities and made publicly available via the European
12 Environmental Agency (EEA). Satellite observations can provide independent and more timely
13 information on NO_x emissions. A new version of the inversion algorithm DECSO (Daily
14 Emissions Constraint by Satellite Observations) has been developed for deriving NO_x
15 emissions for Europe on a daily basis, averaged to monthly mean maps. The estimated
16 precision of these monthly emissions is about 25% for individual grid cells. These satellite-
17 derived emissions from DECSO have been compared to the officially reported European
18 emissions and spatial-temporal disaggregated emission inventories. The country total DECSO
19 NO_x emissions are close to the reported emissions and the emissions compiled by the
20 Copernicus Atmospheric Monitoring Service (CAMS). The comparison of the spatial
21 distributed NO_x emissions of DECSO and CAMS showed that the satellite-derived emissions
22 are often higher in cities, while similar for large power plants and slightly lower in rural areas.

23

24

25 1. Introduction

26 Nitrogen oxides (NO_x) concentrations play an important role in air quality, the nitrogen cycle,
27 and as precursor for climate gasses. Knowledge of NO_x emissions is also important for
28 climate studies (Shindell et al., 2005). Because of the importance of NO_x for air quality, in
29 Europe both the concentrations in air and emissions to air are regulated in Europe. Country
30 total NO_x emissions need to be reported by EU countries as part of the Convention for Long-
31 Range Transboundary Air Pollution (LRTAP, Pinterits et al., 2021) and the National Emission
32 reductions Commitments (NEC) Directive (NEC, 2023) of the European Union. More detailed

33 emission inventories including spatial distribution are compiled based on reported emissions,
34 statistical information (e.g. population density) and activity data. Examples of these
35 inventories on a global scale are the Emissions Database for Global Atmospheric Research
36 (EDGAR, EC-JRC/PBL, 2011, Janssens-Maenhout et al., 2015) and the various global and
37 regional emission inventories developed in the context of the Copernicus Atmosphere
38 Monitoring Service (CAMS, Innes et al, 2019) of the EU Copernicus programme. These gridded
39 emission inventories are widely used for global atmospheric composition and regional air
40 quality modelling. The realism of the air quality model results depends largely on the accuracy
41 of the emission inventory (Thunis et al, 2021).

42 Since the availability of satellites capable of measuring NO₂ concentrations in the atmosphere,
43 methods have been developed to derive top-down emissions (Streets et al., 2013). These top-
44 down emissions have the major advantage that they are based on observations ~~s-based~~. This
45 fully independent source of information provides the possibility to check reported emissions,
46 monitor rapid changes (e.g. due to the COVID-19 lockdowns) and has the potential of finding
47 unknown and unreported sources. Polar orbiting satellites with a global daily coverage within
48 1-3 days, allow monitoring of changes in emissions on timescales of days to weeks. Nadir-
49 viewing S₅ satellites measure total column concentrations of trace gases, and the distinction of
50 source sector type must be deduced via the source location. A popular inversion technique
51 for NO_x emissions is the divergence method of Beirle et al. (2021, 2023), where the average
52 flux is calculated in grid cells, assuming local mass balance, to find the sources of the
53 emissions. Although no model is needed in this method, the required spatial derivations lead
54 to noisy fields for daily overpasses, and it only provides useful emissions when averaged over
55 a longer period. Furthermore, assumptions must be made for the chemical lifetime, and
56 simplifications lead to biases, especially in background emissions. A second class of methods
57 is based on plume fitting (Fioletov et al., 2022). This method can be applied to individual
58 overpasses but needs well-defined plume shapes which is not trivial for areas with multiple
59 sources close together. Both these methods simplify atmospheric transport as two-
60 dimensional. For a full three-dimensional description of transport and chemistry, a data
61 assimilation or inverse modelling method is used to match the model results and observations
62 by adapting the emissions (Miyazaki et al., 2017, Fortems-Cheiney et al., 2021). A typical
63 application of satellite-derived emissions is the study of the impact of recent events, like for
64 example the effect of COVID regulations (Ding et al., 2020). Top-down emissions are also used

65 for the verification and support to improve current emission inventories (Guevara et al., 2021;
66 Crippa et al., 2023). [Guevara et al. \(2021\) and Crippa et al. \(2023\) concluded that interesting](#)
67 [aspects for future studies to study more closely](#) are the spatial distribution, seasonal time
68 profiles and multi-annual trends of the emissions.

69 In this study we present the latest version 6.3 of the Daily Emissions Constrained by Satellite
70 Observations DECSO (DECSO) inversion algorithm. The DECSO algorithm can be applied for
71 the operational monthly (or even daily) monitoring of emissions for any region worldwide
72 based on satellite observations of trace gases such as SO₂, NH₃ or NO₂. In this paper this new
73 DECSO version has been applied to NO₂ observations over Europe from the TROPOMI
74 instrument (Veefkind et al., 2012) on board the Sentinel-5P satellite. The DECSO system is
75 efficient, requires only a single forward run of the chemistry-transport model and takes about
76 12 hours to process one month of data on a 30-core computer. Here, we will evaluate the
77 performance of DECSO on various spatial scales (from national to point sources) by
78 comparison with the various bottom-up emission inventories available for Europe. By
79 comparing satellite derived emissions with bottom-up emissions we gain insight in the
80 accuracy of both derived emission datasets.

81

82

83 **2. Methodology and data**

84

85 **2.1 DECSO: inversion of TROPOMI observations**

86 The inversion algorithm DECSO (Daily Emissions Constrained by Satellite Observations) has
87 been developed at KNMI for the purpose of deriving emissions for short-lived gases (Mijling
88 and van der A, 2012). DECSO is using a Kalman Filter implementation for assimilating
89 emissions. The emission forecast model is based on persistency from the analysis, while the
90 concentrations are calculated from the emissions by a chemical transfer model (CTM) and
91 compared to satellite observations. The sensitivity of concentrations to emissions is calculated
92 from multiple forward trajectories to account for the transport of the short-lived gas, but only
93 a single CTM forward run is needed. More detailed information on the method can be found
94 in Mijling and Van der A (2012), the validation is described in Ding et al. (2017a) and the
95 previous latest published version, i.e. DECSO v5.2, is described in Ding et al. (2020). Recent
96 developments of the algorithm to improve its resolution and quality have led to the release

97 of version 6.3. The most important updates are the use of a recent version of the chemical
98 transport model, improved [use of TROPOMI observations](#) and changes in the sensitivity matrix
99 calculations. [More details of these updates follow below.](#)

100 The chemical transport model in DECSO has been upgraded to the latest version of the
101 Eulerian regional off-line CTM CHIMERE v2020r3 (Menut et al., 2021). The implementation of
102 CHIMERE in DECSO was described in Ding et al. (2017b). In this study CHIMERE is combined
103 with the Copernicus Landcover 2019 data (Buchhorn et al., 2020) and HTAP v3-~~2018~~
104 [\(Hemispheric Transport of Air Pollution, Crippa et al., 2023\) of 2018](#) for the source sector split
105 of the emissions. The meteorological input data for CHIMERE are the operational [ECMWF](#)
106 [\(European Centre for Medium-Range Weather Forecasts \(ECMWF\)\)](#) weather forecasts.

107 The sensitivity matrix, giving the relationship between emissions and concentrations, is based
108 on trajectories calculated with a high temporal resolution ([a time step of maximum](#) 7.5
109 minutes). In the new version the relationship [between emissions and concentrations](#) is limited
110 to a ~~range of~~ maximum [distance of](#) 150 km to avoid effects of errors in the trajectories over
111 longer distances. [With this sensitivity matrix not only observations over the source are](#)
112 [affecting the derived emissions, but also the transported concentrations away from the](#)
113 [source within 150 km.](#) The default settings of DECSO described here are for a grid resolution
114 of 0.2 degree. For higher grid resolutions, the settings for temporal resolution and maximum
115 trajectory distance are increased and reduced respectively.

116 The error parametrizations for the emission model and observations are based on the
117 Observation-minus-Forecast (OmF) and the Observation-minus-Analysis (OmA) statistics of
118 previous runs. The latest version of DECSO can also be applied to ~~the~~ simultaneously
119 optimisation of emissions of NO_x and NH₃ (Ding et al., 2024).

120 [Although HTAP v3 has been used for the sector distribution of emissions and other species in](#)
121 [CHIMERE, no use is made of a -priori \(bottom-up\) NO_x emissions in DECSO. DECSO is using a](#)
122 [persistence forward model in which the emissions of the current day are equal to the](#)
123 [emissions of the previous day. In addition, there is a strong dependency of the calculated](#)
124 [emissions on the observations as shown in Ding et al. \(2021\). Since the derived emissions are](#)
125 [updated by addition and not by multiplication factors, unknown sources or emission changes](#)
126 [are detected fast.](#)

127 [TROPOMI is a spectrometer instrument onboard the Sentinel 5P satellite, which was launched](#)
128 [in October 2017 and is flying a sun-synchronous polar orbit with a local overpass time of 13:30.](#)

129 The measured NO₂ columns are derived from the visible band that has a spectral resolution
130 of 0.54 nm (0.2nm sampling) and a signal-to-noise ratio of about 1500 (van Geffen et al.,
131 2022a). The NO₂ tropospheric columns have a spatial resolution of 5.5 x 7 km (5.5 x 3.5 km
132 since 6 August 2019) over a swath of about 2600 km, which means that global coverage is
133 reached daily.

134 We are using the latest version 2.4 reprocessed and offline TROPOMI NO₂ observations (van
135 Geffen et al,2022b) converted to super-observations as described in Ding et al. (2020). The
136 modelling of NO₂ in the free troposphere, governed by processes like lightning, deep
137 convection, aircraft emissions or long-range transport, is often simplified in regional air-quality
138 models focusing on surface concentrations. However, the TROPOMI NO₂ product is providing
139 a tropospheric column, which includes the Planetary Boundary Layer (PBL) and the free
140 troposphere. As a result, model biases in the free troposphere may be a significant source of
141 systematic error in the model-satellite comparisons (Douros et al., 2023). To mitigate this
142 problem we adapt the TROPOMI NO₂ retrieval by replacing the tropopause level by a 700 hPa
143 level. The stratosphere + free troposphere NO₂ column from the TM5-MP (Tracer Model 5,
144 <https://tm5.site.pro/>, Williams et al., 2017) assimilation system are now subtracted from the
145 satellite-observed total column, and new retrieved layer column amounts, air-mass factors
146 and kernels are computed for the surface to 700 hPa layer in the same way as they are
147 computed for the tropospheric column (van Geffen et al., 2022b). The TROPOMI tropospheric
148 column and averaging kernels have been recomputed by combining the TM5 MP retrieval a-
149 priori model output with the data in the satellite level-2 file. This results in a retrieved partial
150 column from about 700 hPa (terrain following) to the surface. The corresponding averaging
151 kernels are rescaled using the 700hPa column air-mass factor and are zero above the 700 hPa
152 level. This procedure removes NO₂ in the free troposphere caused by, for example, lightning
153 or long-range transport, which is known to be a significant source of error (Douros et al.,
154 2023). The observations with a cloud radiance fraction of more than 50% (this corresponds to
155 a cloud fraction of about 20%) have not been used. For Europe, it means that about 45% of
156 the observations are used.

157 Superobservations (Sekiya et al., 2022) are constructed as the area-weighted mean of cloud-
158 free (qa value > 0.75) TROPOMI observations over the CHIMERE model grid cells. For a grid of
159 0.2x0.2 degree a superobservation contains about 10 to 15 TROPOMI NO₂ observations. The
160 use of superobservations improves the signal-to-noise ratio and it reduces the calculation time

161 of DECSO. On the other hand, the sampling of transported NO₂ from the observations
162 calculated back to the source on the emission grid, based on superobservations, will slightly
163 spread out the derived emissions and reduce their spatial resolution compared to using
164 individual observations. The chosen size of the superobservation grid of 0.2x0.2 degree is
165 therefore a compromise between noise, calculation speed and spatial resolution. Knowing
166 that the smoothing of emissions after averaging can be imagined as a distribution by a pyramid
167 shape weighting function around a point source, a deconvolution is possible for isolated
168 emission sources with a known location. The current version of DECSO makes use of the
169 superobservations software as also used in Sekiya et al. 2022. The software has been further
170 developed focusing on a realistic description of the superobservation uncertainty (Rijsdijk et
171 al, 2024) and this new [superobservation](#) software ~~is planned~~will to be used in future DECSO
172 studies.

173 In a post-processing step, the total monthly NO_x emissions are split into anthropogenic and
174 [\(biogenic\) soil emission](#) contributions [Lin et al. \(2023\)](#). ~~This is based on the assumption~~
175 ~~that~~[The soil biogenic](#) emissions show a strong seasonal cycle with low emissions in winter,
176 while the anthropogenic emissions are more constant over the year. [The soil NO_x emissions](#)
177 [are derived by fitting the monthly emissions in a selection of grid-cells without any significant](#)
178 [anthropogenic contribution according to land-use data. In this way the monthly averaged soil](#)
179 [NO_x emissions in the categories for forest, agricultural and shrub-land are derived. These](#)
180 [monthly soil NO_x emissions are weighted with the land-use type of these 3 categories in each](#)
181 [grid cell and subtracted from the total derived NO_x emissions to end up with the](#)
182 [anthropogenic NO_x emissions discussed in this study.](#) This splitting method is ~~detailed~~
183 described in detail in Lin et al. (2023).

184 For the monthly emissions also the precision of the emission in each grid cell has been
185 calculated. Each daily NO_x emission per grid cell derived by DECSO is accompanied by a
186 standard deviation calculated according the Kalman Filter equations [\(the standard deviation](#)
187 [is part of the emission data product of DECSO\)](#). As the starting point of each daily step in the
188 calculation by DECSO is the emissions of the previous day, the resulting emissions will show
189 an autocorrelation in their errors. For each grid cell the autocorrelation function ρ_k (for time
190 lag k) has been calculated for each month. We see typically that the autocorrelation effects in
191 the errors have disappeared completely after about 1 week.

192 When calculating the variance of the monthly mean values, we must take this autocorrelation
193 function into account. The variance S of the monthly mean NO_x emissions per grid cell is
194 calculated following Bayley and Hammersley (1946) or Box et al. (2008) as

195

$$196 \quad S = \frac{\sigma^2}{n} \left[1 + 2 \sum_{k=1}^{n-1} \left(1 - \frac{k}{n} \right) \rho_k \right] ,$$

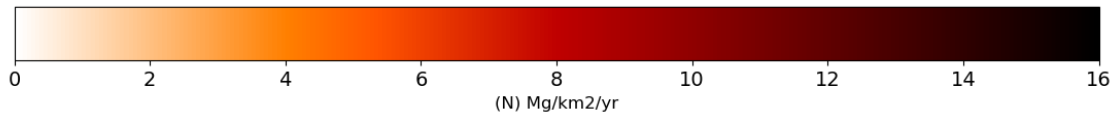
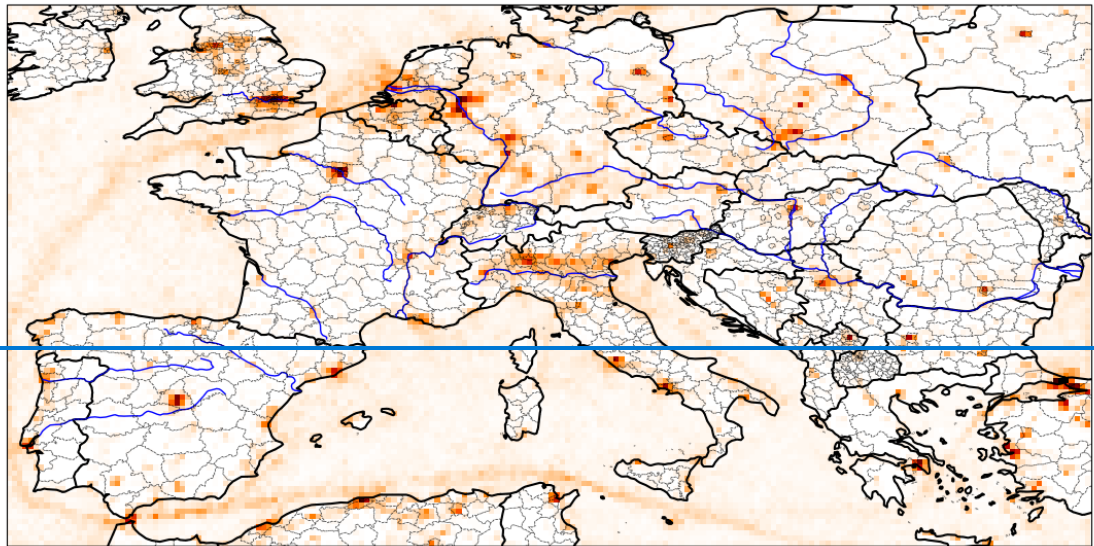
197

198 where σ is the mean standard deviation of the emissions over the month and n is the number
199 of days in the month. We assume here that σ is not varying a lot over the month. This precision
200 σ is calculated in the Kalman equations of the inverse modelling and it depends on the
201 precision of the TROPOMI NO_2 superobservations. The precision depends on the location and
202 emission magnitude, but on average the precision is estimated as 8% for annual emissions,
203 25% for monthly emissions and between 10 and 60 % for the daily emissions.

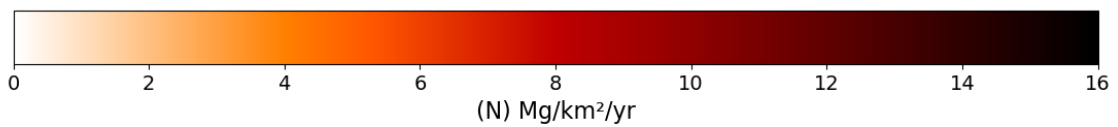
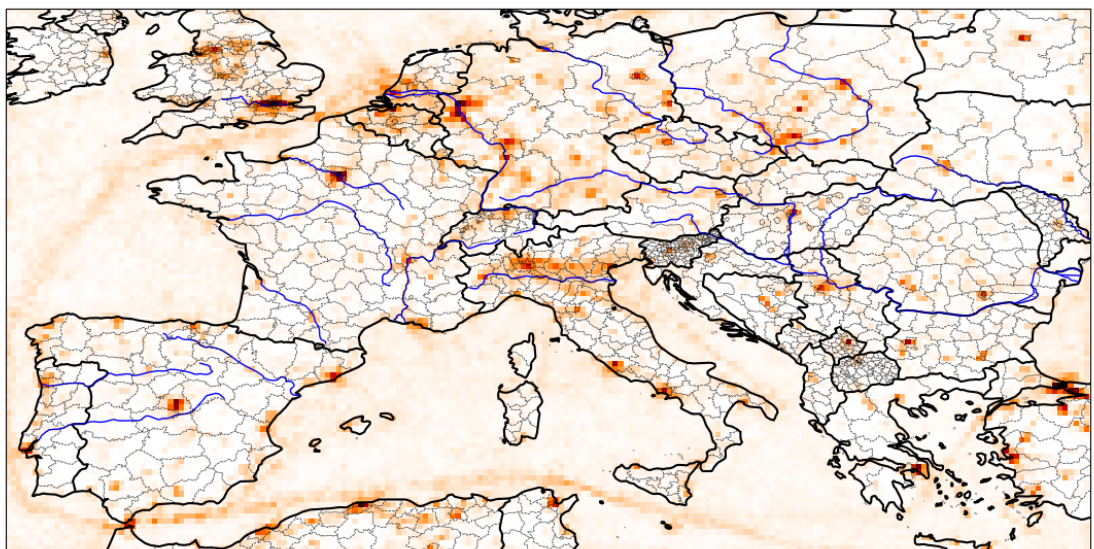
204

205 In this study we will focus only on NO_x emissions. Although DECSO has been applied to many
206 regions in the world, [in this study](#) we will show results for a domain over Europe (35°-55°N, 10°
207 W-30°E) and for 0.2 degree spatial resolution. The temporal resolution of our inversion is daily,
208 usually averaged to monthly or yearly mean values, for the period of 2019 to 2022. Figure 1
209 shows the average annual emissions for 2019 as derived with DECSO version 6.3. [In the Figure](#)
210 [the emissions of major cities and industrial facilities can be identified. Ship emissions show up](#)
211 [clearly in most seas where many ships follow the same route. Other areas over sea appear](#)
212 [noisier since ship locations are moving while emitting \$\text{NO}_x\$. The most polluted regions in](#)
213 [Europe are the densely populated and industrial regions in the Po Valley, the Ruhr area, and](#)
214 [the West of the Netherlands.](#)

215



216



217

218

Figure 1 The annual-averaged anthropogenic NO_x emissions for 2019 derived from TROPOMI NO₂ observations using the DECSO algorithm.

219

220

221

222

2.2 Databases for validation

223

For comparison of the emission results in Europe we will use several inventories, all based on official emissions reported to the European Environmental Agency (EEA). The first one is the

224

225 inventory of national emissions per source category reported under the National Emission
226 reductions Commitments (NEC) Directive of the European Union. Another similar inventory is
227 the Emission inventory reported under the Convention on Long-range Transboundary Air
228 Pollution (LRTAP), which give the country totals of emissions in various source categories. The
229 last one we will use is the European Pollutant Release and Transfer Register (E-PRTR; EPRTR,
230 2012), which is a database of the individual emissions of the biggest industrial facilities (above
231 0.1Mg/year) in Europe. The E-PRTR emissions data are reported on an annual basis. From here
232 on we will call those databases simply NEC, LRTAP and E-PRTR. Besides comparison with these
233 officially reported emissions, we will also compare our emissions to the regional
234 anthropogenic emission inventory CAMS-REG-ANT v5.1 for air quality in Europe (Kuenen et
235 al., 2022) developed for the Copernicus Atmospheric Monitoring Service (CAMS), hereafter
236 called CAMS-REG. For these annual CAMS-REG emissions we use the total emissions regridded
237 from $0.1^\circ \times 0.05^\circ$ to $0.2^\circ \times 0.2^\circ$ and exclude the soil agricultural emissions (i.e. agricultural
238 categories), since soil emissions ~~which~~ are also excluded in DECSO. Temporal profiles are also
239 derived in CAMS, which allow us to compare timeseries for monthly averaged values. We will
240 use the Copernicus Atmosphere Monitoring Service TEMPO profiles (CAMS-GLOB-TEMPO,
241 Guevara et al., 2021,2023) for comparison of monthly variations in anthropogenic NO_x
242 emissions. The global emission data version 5.3, called CAMS-GLOB-TEMPO, on a resolution
243 of $0.1^\circ \times 0.1^\circ$ has been regridded to $0.2^\circ \times 0.2^\circ$ resolution and is hereafter referred to as CAMS-
244 TEMPO.

245

246 **3. Evaluation of the satellite derived emissions**

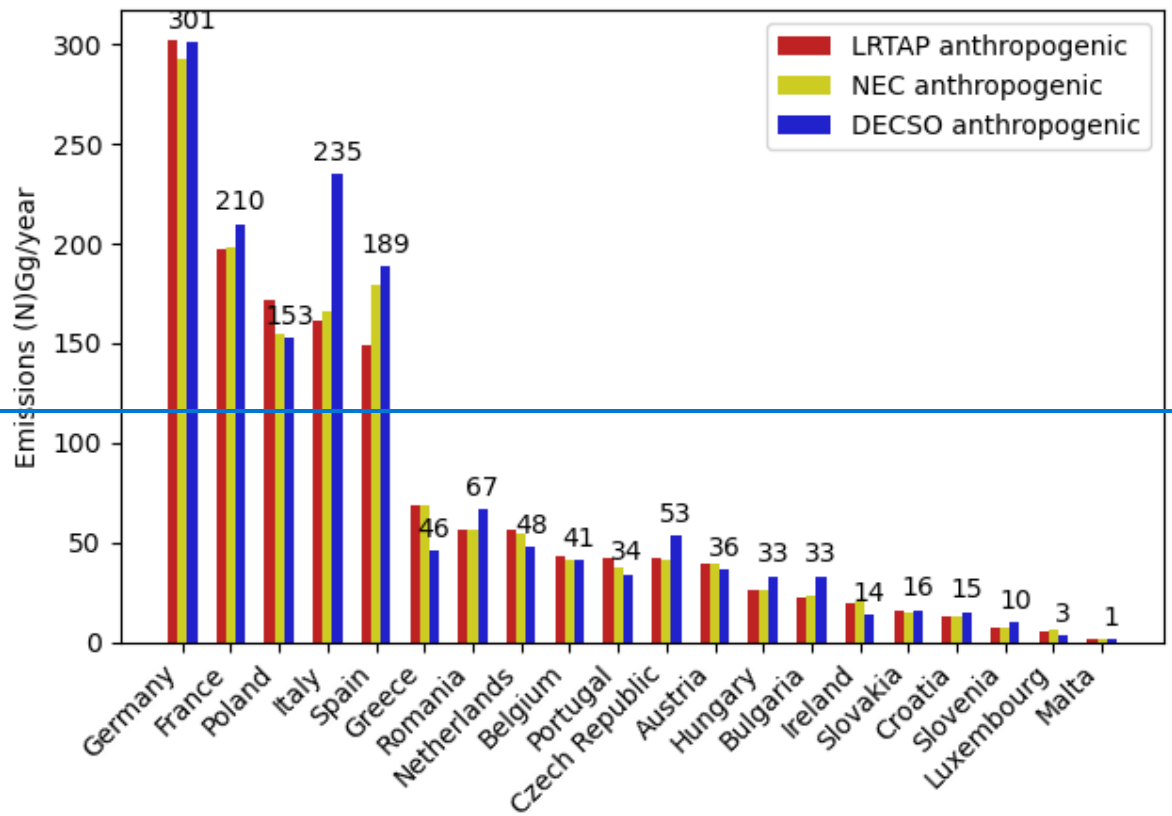
247

248 **3.1 Country scale intercomparison**

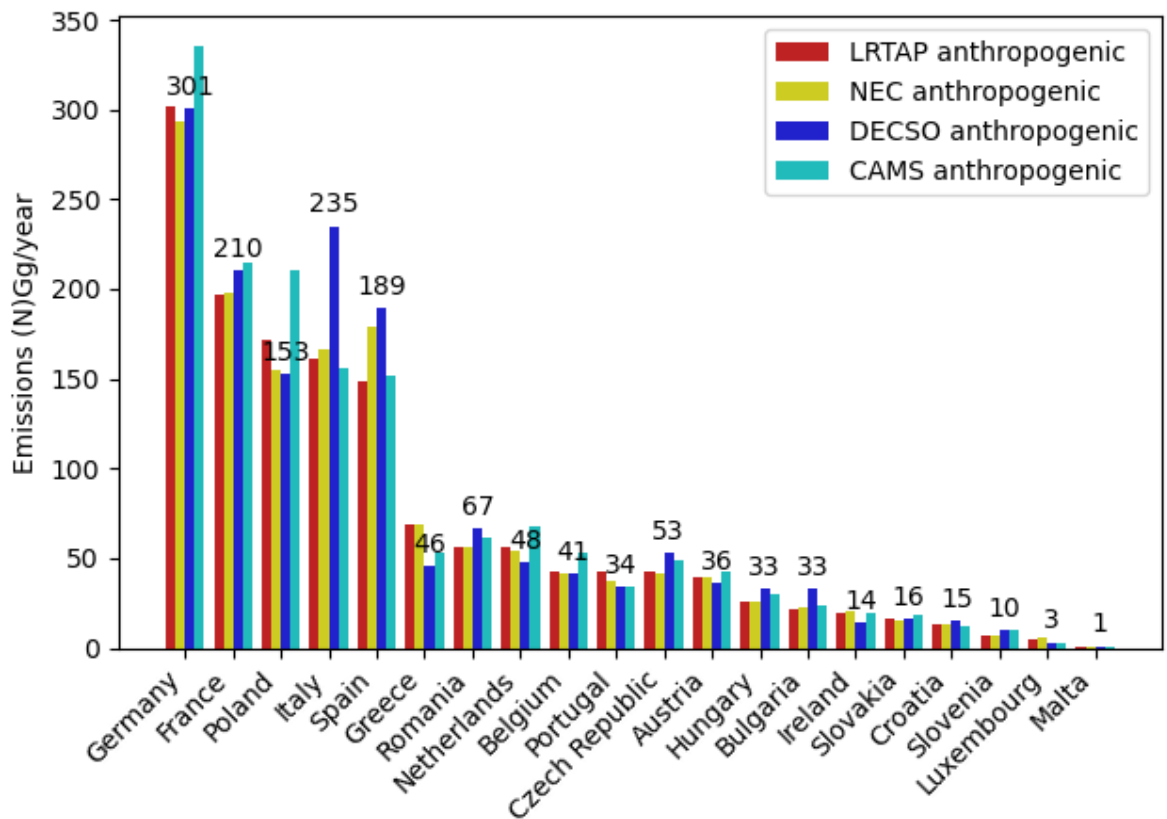
249 The NO_x emissions derived with DECSO have been summed over the countries ~~(weighted by~~
250 ~~the land fraction per grid cell)~~ in our domain and compared to the registered total emissions
251 in NEC and LRTAP. Note that for the national total emissions the spatial resolution or spatial
252 smoothing of the derived emissions play hardly any role. In total 21 countries are completely
253 covered by our geographical domain and have reported their emissions. The total
254 anthropogenic emissions (excluding agricultural-soil emissions) for all these 21 countries are
255 1.44 Tg/year according both LRTAP and NEC. The total calculated anthropogenic emissions by
256 DECSO are 1.54 Tg/year, about 7% higher than the reported emissions. The total

257 anthropogenic emissions of CAMS-REG (excluding ~~agricultural-soil~~ emissions) for the same
258 region are 1.54 Tg/year, in agreement with DECSO. Note that the total soil emissions derived
259 by DECSO are 0.78 Tg/yr for the same region, but this number cannot be compared because
260 soil emissions in LRTAP and NEC are only given for the agricultural sector and not for forestry.
261 The anthropogenic country totals are shown in Figure 2. In general, we see a good agreement
262 with the official reported country total emissions of LRTAP and NEC per country except for
263 Italy, which has much lower reported emissions. Greece, on the other hand, has higher
264 registered emissions, but the mismatch might be related to the difficult counting over the
265 Greek islands, since we have weighted these emissions ~~are weighted~~ by the land fraction in
266 ~~the each~~ grid cells ~~of DECSO~~ to exclude maritime emissions in ~~our counting~~ these country
267 totals. For CAMS-REG we see bigger deviations not only for Italy, but also for Germany, Poland,
268 and Spain. Note that Ireland is only partly in our geographical domain and has therefore lower
269 emissions according to DECSO. Besides the comparison on a national level also on a provincial
270 scale good agreement is found, as has been shown for Catalonia in the EC-project SEEDS
271 Mijling et al. (2023).

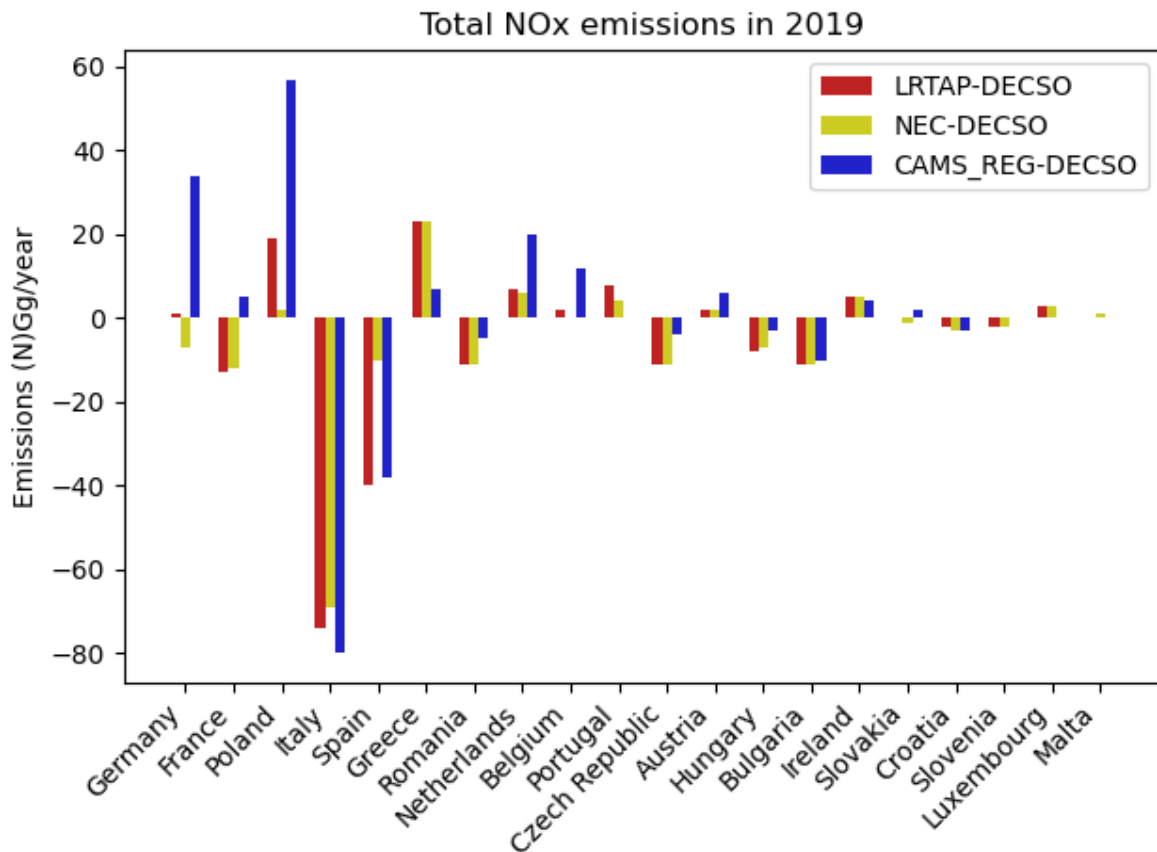
272



273



274



275

276 **Figure 2** (a) Country totals of anthropogenic NO_x emissions (in (N)Gg/year) in the year
 277 2019 according to databases LRTAP₂ and NEC, CAMS-REG and the DECSO calculations. (b)
 278 Differences in total emissions calculated by LRTAP, NEC, CAMS-REG compared to DECSO.

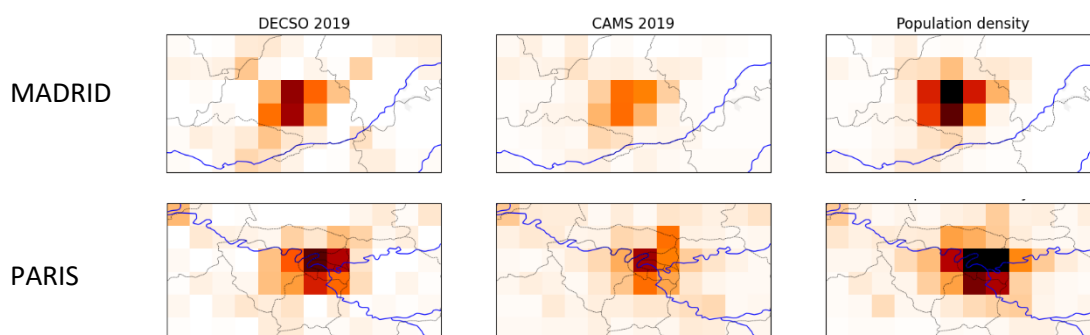
279

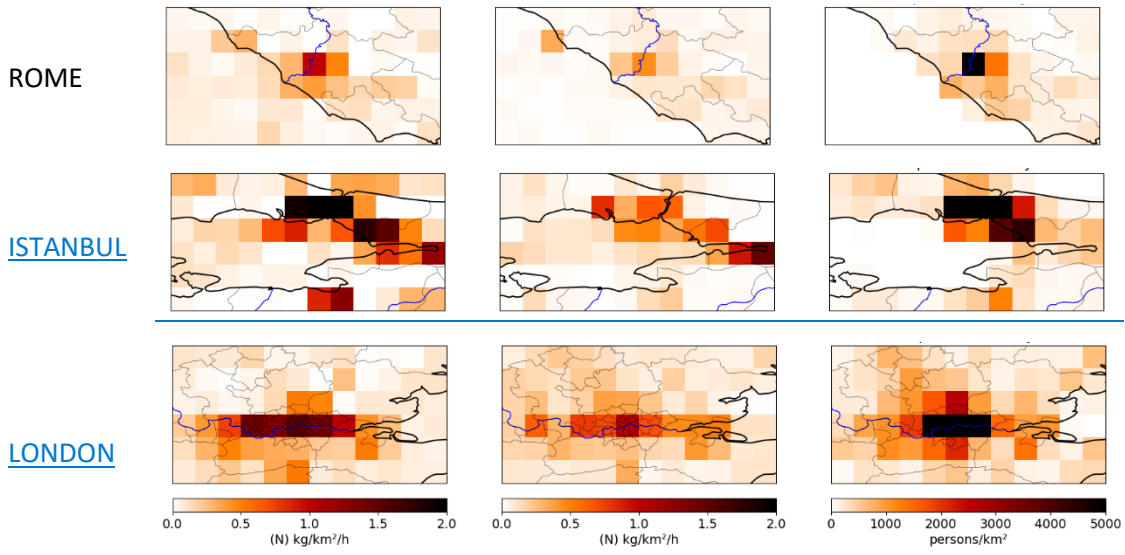
280

281 3.2 City scale

282 With our current spatial resolution of 0.2x0.2 degree, we observe emissions per city district
 283 for [mega-large](#) cities, but the geographical distribution can be slightly blurred by the 0.2 degree
 284 resolution of the TROPOMI superobservations. Figure 3 shows the spatial distribution of the
 285 annual emissions of DECSO and CAMS-REG for three of the largest [mega](#) cities in Europe:
 286 Madrid, Paris, and Rome. Although DECSO show similar emissions for the country totals, we
 287 see that for [megacities-large cities](#) DECSO estimates higher emissions in the city center, and
 288 more activities are seen in the region surrounding the city, as compared to the CAMS-REG
 289 emissions. The industrial complexes at Rouen located north-west of Paris, and at the port of
 290 Civitavecchia located west of Rome are similar in DECSO compared to CAMS-REG. The area of
 291 Rouen used to have an active oil refinery, but in recent years the industrial emissions are about

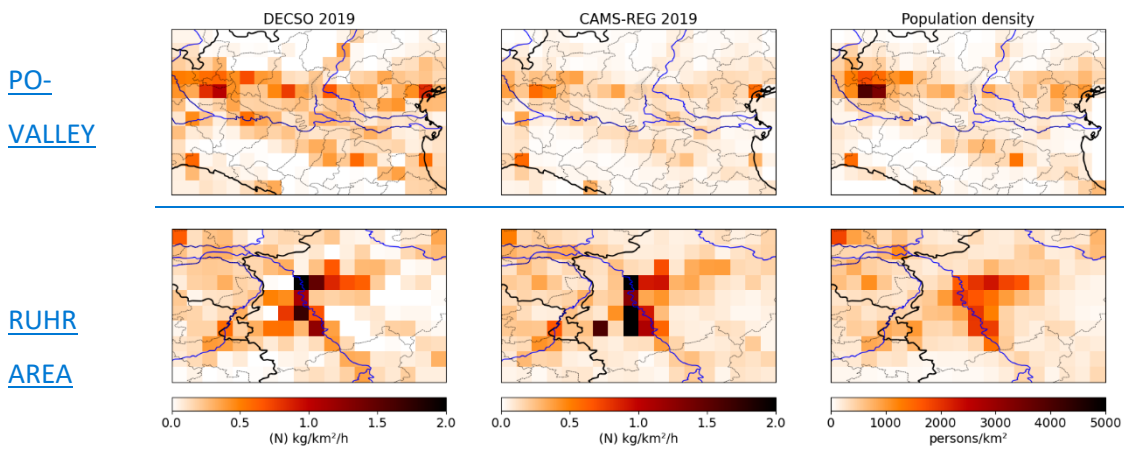
292 0.11 (N)kg/km²/h according to the E-PRTR database, which compares well to CAMS-REG and
 293 DECSO. The spatial extent of high emissions in the Rome area is smaller in CAMS-REG, which
 294 follows more the population density. However, the densely populated center of Rome is
 295 surrounded by a busy ring road with a 20 km radius and a lot of commercial activities around
 296 the city, which are not reflected in the population density map. The two powerplants at
 297 Civitavecchia have reported emissions according to the E-PRTR database, which are equivalent
 298 to about 0.17 (N)kg/km²/h per grid cell, which is closer to the DECSO derived emissions.
 299 Although this study focuses mainly on the land emissions, we see in the map for Rome, that
 300 the maritime emissions of CAMS-REG and DECSO disagree a lot, and this is a topic for further
 301 studies. [The city emissions in Istanbul are much higher in DECSO than in CAMS-REG. These](#)
 302 [emissions will include a lot of ship emissions since it includes the busy ship route through the](#)
 303 [Bosporus Strait. The map of the greater area of London shows that DECSO has higher](#)
 304 [emissions in the city, but lower outside the city. This is a pattern we see in general: in most big](#)
 305 [cities the emissions derived by DECSO show a similar pattern than in CAMS-REG but the](#)
 306 [emissions are higher, the emissions in rural regions on the other hand are usually lower in](#)
 307 [DECSO than in CAMS-REG. The lower emissions in the rural regions can be seen in Figure S1,](#)
 308 [which show maps for Europe of both emission products.](#)
 309 [In Figure 3b we show the emission for two large industrial areas in Europe; the Po-Valley and](#)
 310 [the Ruhr area. For the Po Valley the patterns are similar, but again the DECSO emissions are](#)
 311 [higher in every city except for Genua in the Southeast corner of the map. For the Ruhr area,](#)
 312 [the difference of emissions over the cities is small, the biggest differences are located at the](#)
 313 [big power plants of Weisweiller, Neurath and Niederaussem around the open-pit lignite mine](#)
 314 [of Hambach \(the largest of Europe\). The DECSO emissions are lower than CAMS-REG at the](#)
 315 [locations of these power plants.](#)
 316





317 **Figure 3a** Zoom-in plots for 5 large megacities in Europe to illustrate the differences in
 318 distribution of emissions of DECSO (first column), CAMS-REG (second column) and the
 319 population density (third column) per km².

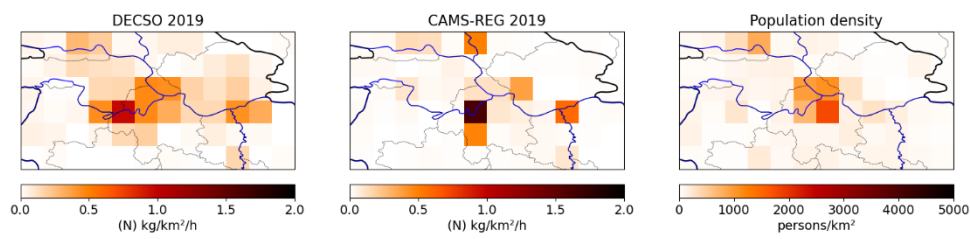
320



321

322 **Figure 3b** Zoom-in plots for two large densely populated and industrial regions in
 323 Europe to illustrate the differences in distribution of emissions of DECSO (first column),
 324 CAMS-REG (second column) and the population density (third column) per km².

325

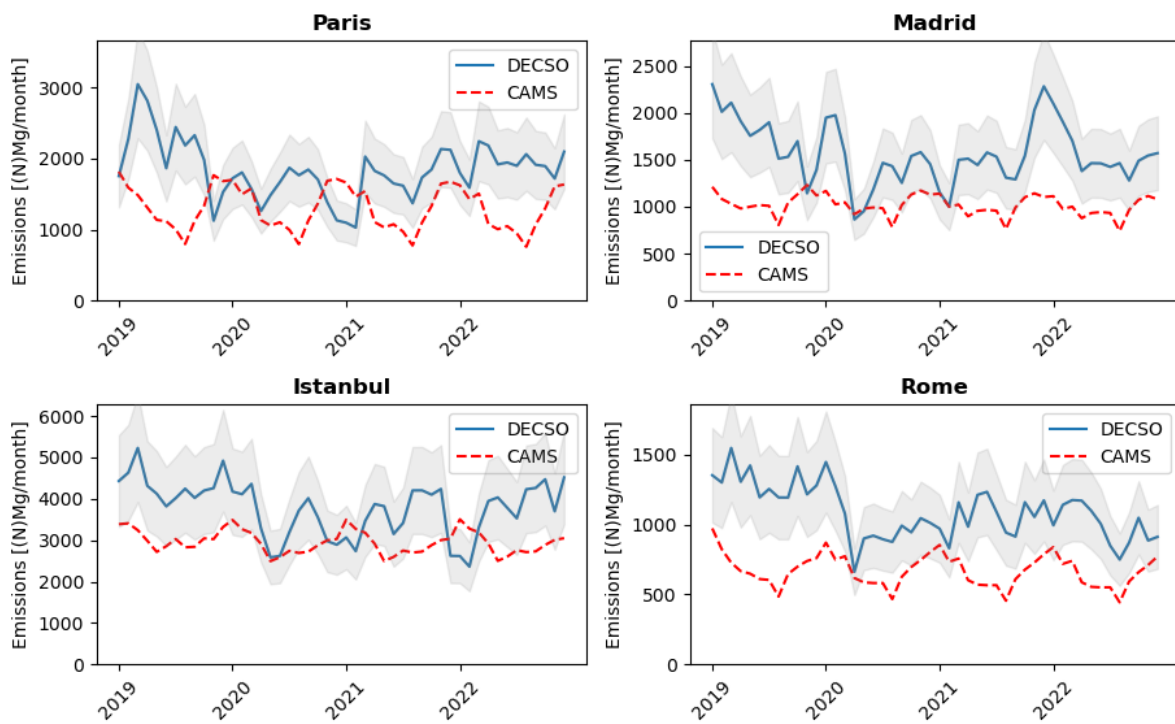


326

327 **Figure 3c** A map of North Serbia with NO_x emissions of DECSO, and CAMS-REG. The
 328 population map shows especially the higher population for Belgrade. The emissions in DECSO
 329 are mainly correlated with the locations of several coal power plants (Nikola Tesla -A, -B, and
 330 -Kolubara) and a cement factory (Lafarge in Beocin) in the North-West.

331
 332 On a European scale the biggest difference between CAMS-REG and DECSO was found for the
 333 region around Belgrade in Serbia (Figure 3c). The city of Belgrade is identified by the higher
 334 population density in Figure 3c. West of the city, the Nicola Tesla power plants are located,
 335 which are strong emitters according to the E-PRTR database. They show up as a strong
 336 emission source in the DECSO emissions, but they are mislocated in the current CAMS-REG
 337 emissions.

338



339
 340 **Figure 4** Timeseries of monthly NO_x emissions derived by DECSO for the cities Paris,
 341 Madrid, Istanbul and Rome in the period 2019 to 2022. The shaded grey area shows the
 342 estimated uncertainty on the DECSO emissions. The dotted red line shows the CAMS-TEMPO
 343 NO_x emissions for the same grid boxes.

344

345 [Figure 4 shows examples of timeseries for city emissions, in this case for the cities of Paris,](#)
346 [Madrid, Istanbul and Rome \(also shown in Figure 3a\). In these plots we report the total](#)
347 [emissions in a square area of 5 by 5 grid cells centred on the city centre to make sure the](#)
348 [whole city has been captured. Figure S1 in the supplement is an example of a timeseries for](#)
349 [city emissions, in this case for the city of Paris. As we had seen earlier, the DECSO emissions](#)
350 [are on average higher than for CAMS-TEMPO, but also the seasonal cycle is different. The NO_x](#)
351 [emissions of CAMS-TEMPO show a seasonal cycle, which is almost identical each year, while](#)
352 [DECSO show larger variations from year-to-year. We see clearly the effect of COVID regulations](#)
353 [in all cities, that started first in March/April 2020 in Europe,The time series show 3 low](#)
354 [emission periods: in Nov. 2019 \(reason unknown\), in April 2020 when COVID hits Europe, and](#)
355 [in the winter of 2020-2021 when strict COVID regulations were again in place. After the](#)
356 [recovery from COVID we see that emissions grow again in 2022 to the level of pre-COVID.The](#)
357 [general overall trend in this 4 year time period varies from city to city, but most cities show a](#)
358 [slightly decreasing trend, partly related to a gradual decrease of emissions from road vehicles](#)
359 [linked to European regulations.](#)

360

361 **3.3 Intercomparison for large point sources**

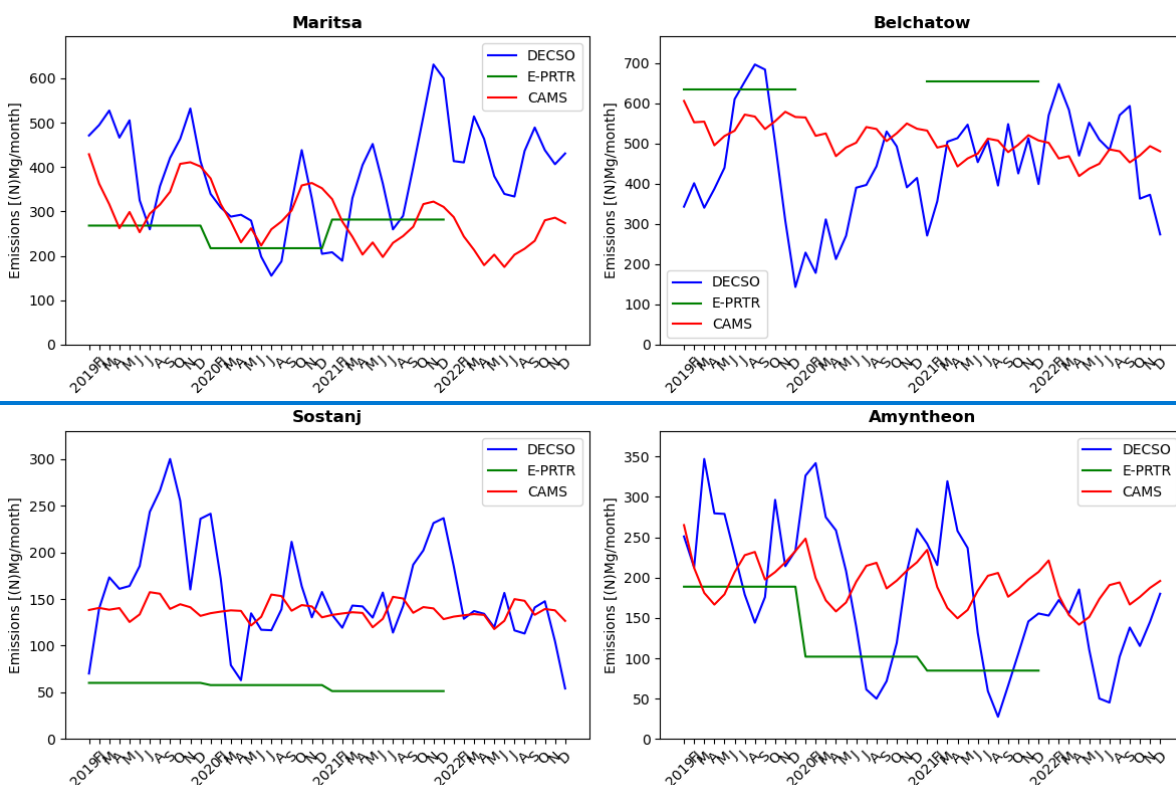
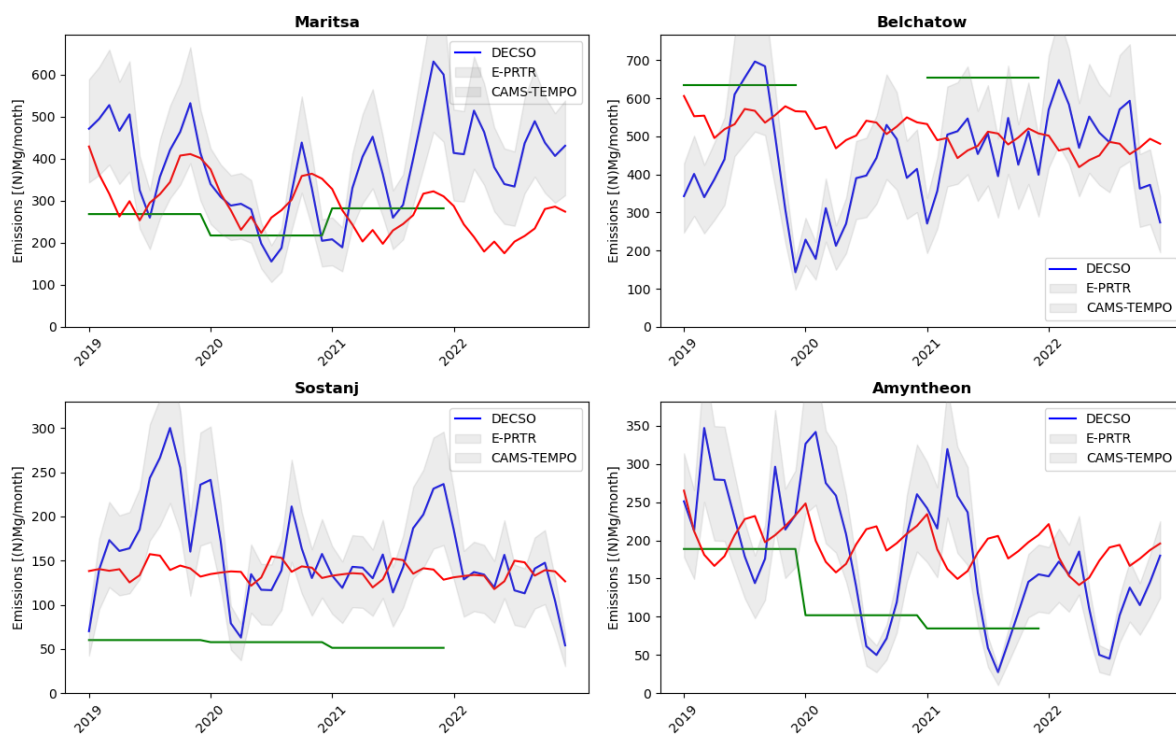
362 To evaluate the performance of monitoring emissions from large point sources (LPS), we
363 compare the DECSO emissions with emissions registered in the E-PRTR data base. The isolated
364 LPS in Europe we selected are all large power plants close to lignite mines. Emissions from
365 DECSO are slightly spread to adjacent grid cells because the spatial resolution of the emission
366 field is less than the sampling of the grid cells as discussed in Sect. 2. To correct for this, we
367 can deconvolute the emissions around the isolated point source, but here we choose to sum
368 the anthropogenic emissions in the 3x3 grid cells including and around the point source to
369 make sure all emissions are accounted for. For the four cases discussed below, no significant
370 other sources exist in these 3x3 grid cell boxes, and [biogenicsoil](#) emissions are excluded. The
371 rural anthropogenic emissions in such an area of 3x3 grid cells in Europe we estimate as about
372 0.13 (N)Gg/year by averaging the emissions of several similar rural 3x3 regions in Europe. We
373 did not correct for this background signal, [but we included this in the error bars of Figure 5-](#)
374 The first case is that of the Maritsa Iztok facility in Bulgaria located next to an open coal mine.
375 There is no big city or any other industrial facility in the [neighborhoodneighbourhood](#), except
376 for the three big power plants of the Maritsa Iztok facility. Figure [4-5](#) shows the monthly

377 averaged emissions calculated by the DECSO algorithm, the CAMS-TEMPO inventory, and the
378 annual emissions from the E-PRTR database for the Maritsa facility. For a fair comparison we
379 selected for CAMS-TEMPO also the same 3x3 grid cells around the LPS. For the period 2019-
380 2022 the annual emissions are given in Table 1 according to DECSO, CAMS-TEMPO and E-PRTR.
381 The difference in annual emissions between DECSO, CAMS-TEMPO and E-PRTR of the Maritsa
382 facility are [relatively small within 20-40 %](#), although DECSO is the highest. The CAMS-TEMPO
383 emissions show a negative trend, which is not visible in DECSO that shows the highest
384 emissions for 2022. Unfortunately, no E-PRTR data for 2022 is yet publicly available.

385 The second power plant is the Bełchatów power plant [in Poland](#) with its capacity of 5,053 MW,
386 the biggest power plant of Europe. It is also one of the most polluting power plants in the
387 world and gets its fuel from the adjacent lignite coal mine of Bełchatów (Guevara et al., 2023).
388 For the year 2020 no emission values are reported in the current E-PRTR database. For the
389 years 2019 and 2021 DECSO observes high emissions of about 5.5 Gg per year, but this is lower
390 than the reported value of more than 7 Gg per year. CAMS-TEMPO also shows lower emissions
391 with a negative trend. Godłowska et al. (2023) showed the stack measurements of this power
392 plant in their Figure 7, which also are in general lower than the E-PRTR values.

393 The next selected isolated power plant is the Šoštanj lignite power plant in the Velenje basin
394 in a mountainous area of Slovenia. It is responsible for one third of the electricity need of
395 Slovenia (Boznar et al., 2012). For this LPS both CAMS-TEMPO and DECSO show more than
396 two times higher emissions than E-PRTR, which is too large to be explained by the small cities
397 or other small sources located in the [neighborhood/ neighbourhood](#).

398 The last case is that of the power plants of the Ptolemais-Amyntheon and Florina coal basins
399 in West Macedonia, Greece, which were also studied by Skoulidou et al. (2021). There are 5
400 power plants associated with and located at this basin, but only three are still active: Agios
401 Dimitrios (1595 MW), Kardias (1200 MW), and Amyntheon (600 MW) (Kostakis, 2009). For
402 2021 no data was reported for Amyntheon in the E-PRTR database. The reported values of the
403 E-PRTR database match those of CAMS-TEMPO and DECSO quite well, except for the year 2020
404 that marks the start of a decrease in emissions in this region. The decreasing trend can be
405 seen in all three emissions time lines, but is strongest in the E-PRTR time series. Most notable
406 in the Figure is the strong seasonal cycle in DECSO NO_x emissions for the Greek power plants
407 with the lowest emissions in summer time. This can be related to the availability of more
408 sustainable energy sources in the summer months.



412 **Figure 45** Timeseries of the NO_x emissions of the selected LPS in Europe as estimated by
 413 DECSO (blue line), E-PRTR (green line) and CAMS-TEMPO (red line). The shaded grey area
 414 shows the estimated uncertainty on the DECSO emissions.

415

416 From this comparison for several large LPS in Europe, we see that CAMS-TEMPO and DECSO
 417 are often larger than the reported emissions in E-PRTR. [In view of the completely different](#)
 418 [methodologies and the estimated precision of 25 % for DECSO monthly emissions,](#) the annual
 419 values of CAMS-TEMPO and DECSO are often in reasonable agreement (within 20%), but the
 420 variability of DECSO is much higher [than of CAMS-TEMPO.](#) [Emissions of thermal power plants](#)
 421 [are more intermittent because of the variability of energy demand and variability in energy](#)
 422 [supply introduced by solar and wind energy sources \(Kubik et al., 2012\).](#) [Note also that CAMS-](#)
 423 [TEMPO has the exact same seasonal variability for each of the 4 years, which seems](#)
 424 [unrealistic.](#) The CAMS-TEMPO emissions in the period 2019 to 2022 show for most studied
 425 LPS a constant negative trend, which was generally not detected in DECSO. Without additional
 426 information it is difficult to draw any conclusions on the performance for LPS, but DECSO
 427 supplies additional information on these industrial facilities in Europe and the largest
 428 discrepancies may be caused by strong diurnal variability (while TROPOMI observes at about
 429 13:30) and will be interesting for further investigation.

430 In all cases we see lower emissions in 2020 during the COVID-19 pandemic. In this period the
 431 demand of energy was lower and while renewable energy output remained similar, the energy
 432 from lignite-based power plants was in relatively less demand (Quitow et al., 2021).

433

434 **Table 1** Annual NO_x emissions (N)Gg/year of the four lignite power plants. [CAMS in](#)
 435 [the table refers to CAMS-TEMPO.](#)

Facility	2019			2020			2021			2022		
	CAMS	DECSO	E-PRTR	CAMS	DECSO	E-PRTR	CAMS	DECSO	E-PRTR	CAMS	DECSO	E-PRTR
	Unit: (N)Gg/yr			Unit: (N)Gg/yr			Unit: (N)Gg/yr			Unit: (N)Gg/yr		
Maritsa	4.1	5.2±0.4	3.2	3.6	3.3±0.3	2.6	3.2	4.6±0.4	3.4	2.8	5.0±0.4	-
Belchatow	6.6	5.5±0.4	7.6	6.3	4.3±0.3	-	5.9	5.4±0.4	7.9	5.6	6.0±0.5	-
Sostanj	1.7	2.4±0.2	0.69	1.7	1.7±0.1	0.66	1.6	1.9±0.2	0.62	1.5	1.3±0.1	-
Amyntheon	2.5	2.8±0.2	2.3	2.4	2.3±0.1	1.2	2.3	2.0±0.2	1.0	1.6	1.3±0.1	-

436

437

438 4. Discussion

439 We presented the latest version of the DECSO algorithm, version 6.3. Updates has been made
 440 for the superobservations, the chemical transport model, the sensitivity matrix and the error
 441 parametrization. The new version [also](#) includes ~~also~~ an error estimate for the monthly NO_x

442 emission data taking into account the autocorrelation in time. The new DECSO version has
443 been applied to the domain of Europe and show more spatial details than before as a result
444 of the higher resolution of TROPOMI observations compared to earlier satellite observations.
445 In the comparison with CAMS-REG over Europe (where emissions are usually well-known) the
446 deviations are small (within 10%) when looking at country scale. For point sources the spread
447 in the differences is much higher, but no systematic effect is yet found. For cities DECSO show
448 higher emissions, while CAMS-REG is higher for rural regions. On a European scale the
449 biggest difference between CAMS-REG and DECSO was found for the region West of Belgrade
450 in Serbia, where the Nicola Tesla power plants are located. While these show up as a strong
451 emission source close to Belgrade in both the DECSO emissions and the E-PRTR database, they
452 are not included or mislocated in the CAMS-REG emissions. This is a prominent example that
453 demonstrates the value of monitoring emissions with satellite observations.

454 The precision of the derived emissions by DECSO are given for each grid cell in the data files.
455 In general, we can say that the precision of NO_x emissions given per grid cell (0.2x0.2 degree)
456 is about 8% for annual emissions, 25% for monthly emissions and between 10 and 60 % for
457 the daily emissions. When averaging over a larger domain the precision will of course become
458 higher by the square root of the number of grid cells.

459 The comparison between CAMS-REG and DECSO [emissions](#) showed that DECSO is very similar
460 [to CAMS-REG for the spatial distribution and the country total on average](#).- While compared
461 to the reported emissions in NEC or LRTAP, DECSO is 7 % higher. Validation of the TROPOMI
462 NO₂ observations showed that, when using averaging kernels, the bias of the tropospheric
463 column is estimated as -8% on average by comparison with MAX-DOAS observations (Keppens
464 and Lambert, 2023). This bias of -8% should result in lower emissions by DECSO and the
465 deviation between DECSO and other inventories would be higher in reality. Keppens and
466 Lambert (2023) further report that for polluted regions the mean bias of the TROPOMI NO₂
467 observations is stronger, about -29%, while for clean areas the median bias is positive and
468 about +13% (when using averaging kernels). This would be contradictory to our findings over
469 cities, where DECSO shows higher emissions than CAMS-REG. Another potential cause of
470 biases in our emissions is the CHIMERE model. More research is needed for a better
471 understanding of the validation results of TROPOMI observations, CHIMERE performance, and
472 the comparisons between DECSO and CAMS.

473 This study shows the potential of DECSO for operational emission monitoring for Europe. The
474 monitoring of LPS ~~only gives mainly clear results~~ is only possible for isolated sources, thus a
475 future n-easy improvement can be ~~gained-made~~ by providing the emissions on a higher
476 resolution at the cost of longer processing time. This will allow the study of more isolated LPS.
477 DECSO has already demonstrated its performance on a 0.1°x0.1° for smaller regions like the
478 Yangtze River Delta (Zhang et al., 2023), West Siberia (van der A et al., 2020), ~~Spain~~ and the
479 Netherlands.

480 In this study the focus was on Europe, but in other regions of the world emissions might be
481 less well-known. For these regions DECSO can or has been applied since we have global
482 satellite observations. Recently we have applied DECSO to areas in Africa, where several mines
483 with high NO_x emissions were found that were unreported in bottom-up emission inventories
484 like EDGAR or CAMS. This shows the possibilities also for application of DECSO in the Global
485 South.

486

487 **Data availability**

488 The TROPOMI NO₂ data version 2.4 are available via the Copernicus website

489 <https://dataspace.copernicus.eu/> and via the TEMIS website

490 <https://www.temis.nl/airpollution/no2.php> (<https://doi.org/10.5270/S5P-9bnp8q8>).

491 The NO_x emissions of DECSO v6.3 are available on the GlobEmission website:

492 https://www.temis.nl/emissions/region_europe/datapage_nox.php.

493 The European emissions data sets for countries NEC, LRTAP and large facilities E-PRTR are available
494 on the website <https://www.eea.europa.eu/en/analysis/> of the EEA.

495 The CAMS databases CAMS-REG-ANT v5.1 and CAMS-GLOB-TEMPO v3.1 are available on the ECCAD
496 website on respectively <https://eccad.sedoo.fr/#/metadata/608/> and-

497 <https://eccad.sedoo.fr/#/metadata/504/> (DOI:10.24380/ks45-9147).

498

499 **Author contributions**

500 RA and JD made the improvements to DECSO, HE developed the superobservation code. RA
501 did the processing, visualisations and main writing. JD and HE reviewed and edited the
502 manuscript.

503

504 **Competing interests**

505 The authors declare that they have no conflict of interest.

506

507 **Acknowledgments**

508 This research was part of the Sentinel EO-based Emission and Deposition Service (SEEDS,
509 Grant ID 101004318) project that has received funding from the European Union's Horizon
510 2020 research and innovation programme. Sentinel-5 Precursor is a European Space Agency
511 (ESA) mission on behalf of the European Commission. The TROPOMI payload is a joint
512 development by ESA and the Netherlands Space Office. The Sentinel-5 Precursor ground
513 segment development has been funded by ESA and with national contributions from the
514 Netherlands, Germany, and Belgium. This work contains modified Copernicus Sentinel-5P
515 TROPOMI data (2018–2023), processed locally at KNMI.

516

517

518

519 **References**

520 Bayley, G. V., & Hammersley, J. M. (1946). The “Effective” Number of Independent Observations in an
521 Autocorrelated Time Series. Supplement to the Journal of the Royal Statistical Society, 8(2), 184-197,
522 <https://doi.org/10.2307/2983560>

523 Beirle, S., Borger, C., Dörner, S., Eskes, H., Kumar, V., de Laat, A., and Wagner, T.: Catalog of NO_x emissions from
524 point sources as derived from the divergence of the NO₂ flux for TROPOMI, Earth Syst. Sci. Data, 13, 2995-3012,
525 <https://doi.org/10.5194/essd-13-2995-2021>, 2021.

526 Beirle, S., Borger, C., Jost, A., and Wagner, T.: Improved catalog of NO_x point source emissions (version 2), Earth
527 Syst. Sci. Data, 15, 3051–3073, <https://doi.org/10.5194/essd-15-3051-2023>, 2023.

528 Box, Jenkins, Reinsel, Time Series Analysis: Forecasting and Control, 4th Ed. Wiley (2008), ISBN 978-0-470-
529 27284-8, p.30.

530 Božnar, M.Z., Mlakar, P., Grašič, B. and Tinarelli, G. (2012), Environmental impact assessment of a new thermal
531 power plant Šoštanj Block 6 in highly complex terrain, Int. J. Environment and Pollution, Vol. 48, Nos. 1/2/3/4,
532 pp.136–144.

533 Buchhorn, M. ; Smets, B. ; Bertels, L. ; De Roo, B. ; Lesiv, M. ; Tsendbazar, N. - E. ; Herold, M. ; Fritz, S,
534 Copernicus Global Land Service: Land Cover 100m: collection 3: epoch 2019: Globe, 2020, DOI:
535 10.5281/zenodo.3939050

536 Crippa, M., Guizzardi, D., Butler, T., Keating, T., Wu, R., Kaminski, J., Kuenen, J., Kurokawa, J., Chatani, S.,
537 Morikawa, T., Pouliot, G., Racine, J., Moran, M. D., Klimont, Z., Manseau, P. M., Mashayekhi, R., Henderson, B.

538 H., Smith, S. J., Suchyta, H., . . . Foley, K. (2023). The HTAP_v3 emission mosaic: merging regional and global
539 monthly emissions (2000–2018) to support air quality modelling and policies. *Earth Syst. Sci. Data*, 15(6), 2667-
540 2694. <https://doi.org/10.5194/essd-15-2667-2023>

541 Ding, J., Miyazaki, K., van der A, R.J., Mijling, B., Kurokawa, J., Cho, S., Janssens-Maenhout, G., Zhang, Q., Liu, F.,
542 and Levelt, P.F., Intercomparison of NO_x emission inventories over East Asia, *Atm. Chem. Phys.*, 2017a, 17,
543 10125-10141, doi.org/10.5194/acp-17-10125-2017

544 Ding, J., R.J. van der A, B. Mijling and P.F. Levelt, Space-based NO_x emission estimates over remote regions
545 improved in DECSO, *Atmospheric Measurement Techniques*, 2017b, 10, 925-938, [doi:10.5194/amt-10-925-](https://doi.org/10.5194/amt-10-925-2017)
546 2017.

547 Ding, J., van der A, R. J., Eskes, H. J., Mijling, B., Stavrou, T., van Geffen, J. H. G. M., Veefkind, J.P., NO_x
548 emissions reduction and rebound in China due to the COVID-19 crisis, *Geophysical Research Letters*, 46,
549 e2020GL089912. <https://doi.org/10.1029/2020GL089912>, 2020.

550 Ding et al., NH₃ emissions from CrIS observations using DECSO, in preparation, 2024

551 Douros, J., Eskes, H., van Geffen, J., Boersma, K. F., Compernelle, S., Pinardi, G., Blechschmidt, A.-M., Peuch, V.-
552 H., Colette, A., and Veefkind, P.: Comparing Sentinel-5P TROPOMI NO₂ column observations with the CAMS
553 regional air quality ensemble, *Geosci. Model Dev.*, 16, 509–534, <https://doi.org/10.5194/gmd-16-509-2023>,
554 2023.

555 EC-JRC/PBL, European Commission, Joint Research Centre (JRC)/Netherlands Environmental Assessment
556 Agency (PBL): Emission Database for Global Atmospheric Research (EDGAR), release EDGAR version 4.2,
557 available at: <http://edgar.jrc.ec.europa.eu/overview.php?v=42>, 2011.

558 EPTR: European Pollutant Transfer Register, database version v4.2, available at: <http://prtr.ec.europa.eu/> (last
559 access: 5 September 2023), 2012.

560 Fioletov, V., McLinden, C. A., Griffin, D., Krotkov, N., Liu, F., and Eskes, H.: Quantifying urban, industrial, and
561 background changes in NO₂ during the COVID-19 lockdown period based on TROPOMI satellite observations,
562 *Atmos. Chem. Phys.*, 22, 4201–4236, <https://doi.org/10.5194/acp-22-4201-2022>, 2022.

563 Fortems-Cheiney, A., Broquet, G., Pison, I., Saunois, M., Potier, E., Berchet, A., et al. (2021). Analysis of the
564 anthropogenic and biogenic NO_x emissions over 2008–2017: Assessment of the trends in the 30 most
565 populated urban areas in Europe. *Geophysical Research Letters*, 48, e2020GL092206.
566 <https://doi.org/10.1029/2020GL092206>

567 Guevara, M., Jorba, O., Tena, C., Denier van der Gon, H., Kuenen, J., Elguindi, N., Darras, S., Granier, C., and
568 Pérez García-Pando, C.: Copernicus Atmosphere Monitoring Service TEMPORal profiles (CAMS-TEMPO): global
569 and European emission temporal profile maps for atmospheric chemistry modelling, *Earth Syst. Sci. Data*, 13,
570 367–404, <https://doi.org/10.5194/essd-13-367-2021>, 2021.

571 Guevara, M., Enciso, S., Tena, C., Jorba, O., Dellaert, S., Denier van der Gon, H., and Pérez García-Pando, C.: A
572 global catalogue of CO₂ emissions and co-emitted species from power plants at a very high spatial and
573 temporal resolution, *Earth Syst. Sci. Data Discuss.* [preprint], <https://doi.org/10.5194/essd-2023-95>, in review,
574 2023.

575 Godłowska, J., M. J. Hajto, B. Lapeta, K. Kaszowski, The attempt to estimate annual variability of NO_x emission
576 in Poland using Sentinel-5P/TROPOMI data, *Atmospheric Environment*, Vol. 294, 2023, 119482,
577 <https://doi.org/10.1016/j.atmosenv.2022.119482>.

578 Inness, A., Ades, M., Agustí-Panareda, A., Barré, J., Benedictow, A., Blechschmidt, A.-M., Dominguez, J. J.,
579 Engelen, R., Eskes, H., Flemming, J., Huijnen, V., Jones, L., Kipling, Z., Massart, S., Parrington, M., Peuch, V.-H.,
580 Razinger, M., Remy, S., Schulz, M., and Suttie, M.: The CAMS reanalysis of atmospheric composition, *Atmos.*
581 *Chem. Phys.*, 19, 3515–3556, <https://doi.org/10.5194/acp-19-3515-2019>, 2019.

582 Janssens-Maenhout, G., Crippa, M., Guizzardi, D., Dentener, F., Muntean, M., Pouliot, G., Keating, T., Zhang, Q.,
583 Kurokawa, J., Wankmüller, R., Denier van der Gon, H., Kuenen, J. J. P., Klimont, Z., Frost, G., Darras, S., Koffi, B.,
584 and Li, M. HTAP_v2.2: a mosaic of regional and global emission grid maps for 2008 and 2010 to study
585 hemispheric transport of air pollution *Atmos. Chem. Phys.* 15, 11411-11432, 2015

586 Keppens, A. and Lambert, J.-C. (editors), Quarterly Validation Report of the Copernicus Sentinel-5 Precursor
587 Operational Data Products #19: April 2018 – May 2023, S5P-MPC-IASB-ROCVR-19.01.00-20230703, version
588 19.01.00 3 July 2023, (available at <https://mpc-vdaf.tropomi.eu/>).

589 Kostakis, G., Characterization of the fly ashes from the lignite burning power plants of northern Greece based
590 on their quantitative mineralogical composition, *Journal of Hazardous Materials*, Vol. 166, 2009, Pages 972-
591 977, <https://doi.org/10.1016/j.jhazmat.2008.12.007>.

592 [Kubik, M.L., P.J. Coker, C. Hunt, The role of conventional generation in managing variability, Energy Policy, Vol.](#)
593 [50, 2012, Pages 253-261, https://doi.org/10.1016/j.enpol.2012.07.010.](#)

594 Kuenen, J., Dellaert, S., Visschedijk, A., Jalkanen, J.-P., Super, I., and Denier van der Gon, H.: CAMS-REG-v4: a
595 state-of-the-art high-resolution European emission inventory for air quality modelling, *Earth Syst. Sci. Data*, 14,
596 491–515, <https://doi.org/10.5194/essd-14-491-2022>, 2022.

597 Lin, X., R. J. van der A, J. de Laat, V. Huijnen, B. Mijling, J. Ding, H. Eskes, J. Douros, M. Liu, X. Zhang, Z. Liu,
598 European soil NO_x emissions derived from satellite NO₂ observations. *ESS Open Archive* . December 10, 2023.

599 Menut, L., Bessagnet, B., Khvorostyanov, D., Beekmann, M., Blond, N., Colette, A., Coll, I., Curci, G., Foret, G.,
600 Hodzic, A., Mailler, S., Meleux, F., Monge, J.-L., Pison, I., Siour, G., Turquety, S., Valari, M., Vautard, R., and
601 Vivanco, M. G.: CHIMERE 2013: a model for regional atmospheric composition modelling, *Geosci. Model Dev.*,
602 6, 981–1028, <https://doi.org/10.5194/gmd-6-981-2013>, 2013.

603 Menut, L., B. Bessagnet, R. Briant, A. Cholakian, F. Couvidat, S. Mailler, R. Pennel, G. Siour, P. Tuccella, S.
604 Turquety, and M. Valari. 2021. ‘The CHIMERE v2020r1 online chemistry-transport model’, *Geosci. Model Dev.*,
605 14: 6781-811.

606 Miyazaki, K., Eskes, H., Sudo, K., Boersma, K. F., Bowman, K., and Kanaya, Y.: Decadal changes in global surface
607 NO_x emissions from multi-constituent satellite data assimilation, *Atmos. Chem. Phys.*, 17, 807-837,
608 doi:10.5194/acp-17-807-2017, 2017.

609 Mijling, B. and R.J. van der A, Using daily satellite observations to estimate emissions of short-lived air
610 pollutants on a mesoscopic scale, *J. Geophys. Res.*, 117, 2012, doi:10.1029/2012JD017817

611 Mijling et al., in preparation, 2024

612 Pinterits, M., B. Ullrich, T. Bartmann and M. Gager, European Union emission inventory report 1990-2019
613 under the UNECE Convention on Long-range Transboundary Air Pollution (Air Convention), EEA Report No
614 5/2021, 2021NEC, Air pollution in Europe: 2023 reporting status under the National Emission reduction
615 Commitments Directive, 2023 ([https://www.eea.europa.eu/publications/national-emission-reduction-](https://www.eea.europa.eu/publications/national-emission-reduction-commitments-directive-2023/air-pollution-in-europe-2023)
616 [commitments-directive-2023/air-pollution-in-europe-2023](https://www.eea.europa.eu/publications/national-emission-reduction-commitments-directive-2023/air-pollution-in-europe-2023))

617 Quitzow, R., G. Bersalli, L. Eicke, J. Jahn, J. Lilliestam, F. Lira, A. Marian, D. Süsser, S. Thapar, S. Weko, S. Williams,
618 B. Xue, The COVID-19 crisis deepens the gulf between leaders and laggards in the global energy transition,
619 *Energy Research & Social Science*, Vol. 74, 2021, 101981, <https://doi.org/10.1016/j.erss.2021.101981>.

620 Rijdsdijk, P., H.J. Eskes, A. Dingmans, K.F. Boersma, T. Sekiya, K. Miyazaki, and S. Houweling, Constructing
621 superobservations from satellite NO₂ for assimilation and model evaluation, preprint 2024.

622 Sekiya, T., Miyazaki, K., Eskes, H., Sudo, K., Takigawa, M., and Kanaya, Y.: A comparison of the impact of
623 TROPOMI and OMI tropospheric NO₂ on global chemical data assimilation, *Atmos. Meas. Tech.*, 15, 1703–
624 1728, <https://doi.org/10.5194/amt-15-1703-2022>, 2022.

625 Shindell, D. T., Faluvegi, G., Bell, N., and Schmidt, G. A. (2005), An emissions-based view of climate forcing by
626 methane and tropospheric ozone, *Geophys. Res. Lett.*, 32, L04803, doi:[10.1029/2004GL021900](https://doi.org/10.1029/2004GL021900)

627 Skoulidou, I.; Koukouli, M.-E.; Segers, A.; Manders, A.; Balis, D.; Stavrakou, T.; van Geffen, J.; Eskes, H. Changes
628 in Power Plant NO_x Emissions over Northwest Greece Using a Data Assimilation Technique. *Atmosphere* 2021,
629 12, 900. <https://doi.org/10.3390/atmos12070900>

630 Streets, D.G., Canty T., Carmichael, G.R., de Foy B., Dickerson, R.R. Duncan, B.N., Edwards, D.P., Haynes, J.A.,
631 Henze, D.K., Houyoux, M.R., Jacob, D.J., Krotkov, N.A., Lamsal, L.N., Liu, Y., Lu, Z., Martin, R.V., Pfister G.G.,
632 Pinder R.W., Salawitch R.J., Wecht, K.J., Emissions estimation from satellite retrievals: A review of current
633 capability, *Atmospheric Environment*, 77, 2013, 1011-1042, <https://doi.org/10.1016/j.atmosenv.2013.05.051>.

634 Thunis, P., M. Crippa, C. Cuvelier, D. Guizzardi, A. de Meij, G. Oreggioni, E. Pisoni, Sensitivity of air quality
635 modelling to different emission inventories: A case study over Europe, *Atmospheric Environment: X*, Volume
636 10, 2021, <https://doi.org/10.1016/j.aeaoa.2021.100111>.

637 van der A, R.J., de Laat, A.T.J., Ding, J., Eskes, H.J., Connecting the dots: NO_x emissions along a West Siberian
638 natural gas pipeline, *npj Clim Atmos Sci* 3, 16, <https://doi.org/10.1038/s41612-020-0119-z>, 2020

639 van Geffen, J. H. G. M., Eskes, H. J., Compernelle, S., Pinardi, G., Verhoelst, T., Lambert, J.-C., Sneep, M., ter
640 Linden, M., Ludewig, A., Boersma, K.F. and Veefkind, J.P.: Sentinel-5P TROPOMI NO₂ retrieval: impact of version
641 v2.2 improvements and comparisons with OMI and ground-based data, *Atmos. Meas. Tech.*, 15, 2037-2060.
642 <https://doi.org/10.5194/amt15-2037-2022>, 2022a.

643 van Geffen, J. H. G. M., Eskes, H. J., Boersma, K. F. and Veefkind, J. P.: TROPOMI ATBD of the total and
644 tropospheric NO₂ data products, Report S5P-KNMI-L2-0005-RP, version 2.4.0, 202207-11, KNMI, De Bilt, The
645 Netherlands, <http://www.tropomi.eu/data-products/nitrogen-dioxide/> (last access: 06 Dec. 2022), 2022b

646 Veefkind, J.P., Aben, I., McMullan, K., Förster, H., Vries, J., de Otter, G., Claas, J., Eskes, H.J., Haan, J.F. de,
647 Kleipool, Q., Weele, M. van, Hasekamp, O., Hoogeveen, R., Landgraf, J., Snel, R., Tol, P., Ingmann, P., Voors, R.,
648 Kruizinga, B., Vink, R., Visser, H., Levelt, P.F., 2012. TROPOMI on the ESA Sentinel-5 Precursor: a GMES mission
649 for global observations of the atmospheric composition for climate, air quality and ozone layer applications.
650 *Rem. Sens. Environ.* 120, 70–83. <https://doi.org/10.1016/j.rse.2011.09.027>.

651 [Williams, J. E., Boersma, K. F., Le Sager, P., and Verstraeten, W. W.: The high-resolution version of TM5-MP for](#)
652 [optimized satellite retrievals: description and validation, *Geosci. Model Dev.*, 10, 721–750,](#)
653 <https://doi.org/10.5194/gmd-10-721-2017>, 2017.

654 Zhang, X., van der A, R., Ding, J., Zhang, X., and Yin, Y., Significant contribution of inland ships to the total NO_x
655 emissions along the Yangtze River, *Atmos. Chem. Phys.*, 23, 5587–5604, [https://doi.org/10.5194/acp-23-5587-](https://doi.org/10.5194/acp-23-5587-2023)
656 2023, 2023.

657

658